Appendix

Higher-order oligomerization promotes localization of SPOP to liquid nuclear speckles

Melissa R. Marzahn[1,†], Suresh Marada[2,†], Jihun Lee[1], Amanda Nourse[3], Sophia Kenrick[4], Huaying Zhao[5], Gili Ben-Nissan[6], Regina-Maria Kolaitis[2], Jennifer L. Peters[7], Stanley Pounds[8], Wesley J. Errington[9,#], Gilbert G. Privé[9,10], J. Paul Taylor[11], Michal Sharon[6], Peter Schuck[5], Stacey K. Ogden[2,*], and Tanja Mittag[1,*]

[1]Department of Structural Biology, St. Jude Children's Research Hospital, Memphis, TN 38105, USA; [2]Department of Cell and Molecular Biology, St. Jude Children's Research Hospital, Memphis, TN 38105, USA; [3]Molecular Interaction Analysis Shared Resource, St. Jude Children's Research Hospital, Memphis, TN 38105, USA; [4]Wyatt Technology Corporation, Santa Barbara, CA 93117, USA; [5]Dynamics of Macromolecular Assembly Section, Laboratory of Cellular Imaging and Macromolecular Biophysics, National Institute of Biomedical Imaging and Bioengineering, National Institutes of Health, Bethesda, MD 20892, USA; [6]Department of Biological Chemistry, Weizmann Institute of Science, Rehovot 7610001, Israel; [7]Department of Cellular Imaging Shared Resource, St. Jude Children's Research Hospital, Memphis, TN 38105, USA; [8]Department of Biostatistics, St. Jude Children's Research Hospital, Memphis, TN 38105, USA; [9]Department of Biochemistry, University of Toronto, Toronto, Ontario M5S 1AB, Canada; [10]Princess Margaret Cancer Centre, Toronto, Ontario M5G 1L7, Canada; [11]Howard Hughes Medical Institute, Department of Cell and Molecular Biology, St. Jude Children's Research Hospital, Memphis, TN 38105, USA

[#] Current address: Department of Biomedical Engineering, University of Minnesota, Minneapolis, MN 55455

[†] These authors contributed equally to this study.

* Corresponding author: Tel: +1-901-595-6281; Email: stacey.ogden@stjude.org;
* Corresponding author: Tel: +1-901-595-6261; Email: tanja.mittag@stjude.org

Running title: Oligomerization promotes SPOP localization

Keywords: isodesmic self-association / membrane-less organelle / prostate cancer / speckle-type POZ protein / ubiquitin ligase

Content

Appendix Table S1: Transfection efficiency of pcDNA-HA-SPOP in NIH 3T3 cells

	HA positive-cells	Total cells	Percentage of HA-positive cells
Image field #1	49	827	5.9
Image field #2	75	1048	7.2
Image field #3	86	805	10.7
Image field #4	68	915	7.4
Image field #5	55	815	6.8
total			**7.6 ± 1.6** [b]

[a] Example of an transfected cell shown in Figure 2A.
[b] The average and standard deviation from five independent wide-field images is given.

Appendix Table S2: Transfection efficiency of pcDNA-GFP-Gli3$^{1-455}$ in NIH 3T3 cells[a]

	GFP positive-cells	Total cells	Percentage of GFP-positive cells
Image field #1	51	223	22.9
Image field #2	103	392	26.3
Image field #3	84	419	20.1
Image field #4	83	309	26.9
Image field #5	81	347	23.3
total			**23.9 ± 2.5** [b]

[a] Example of an transfected cell shown in Figure 2B.
[b] The average and standard deviation from five independent wide-field images is given.

Appendix Table S3: Transfection efficiencies of pcDNA-GFP-Gli3$^{1-455}$ and pcDNA-HA-SPOP in double-transfected NIH 3T3 cells[a]

	GFP pos	HA pos	Double pos	Total cells	% GFP pos	% HA pos	% double pos
Image #1	43	35	33	602	7.1	5.8	5.5
Image #2	45	32	27	608	7.4	5.3	4.4
Image #3	43	36	29	845	5.1	4.3	3.4
Image #4	39	32	27	749	5.2	4.3	3.6
Image #5	48	49	35	531	9.0	9.2	6.6
total					**6.8 ± 1.5** [b,c]	**5.8 ± 1.8** [b,d]	**4.7 ± 1.2** [b]

[a] Example of a double-transfected cell shown in Figure 2C.
[b] The average and standard deviation from five independent wide-field images is given.
[c] 69.5 % of GFP-positive cells are also HA-positive.
[d] 81.7 % of HA-positive cells are also GFP-positive.

Appendix Figures

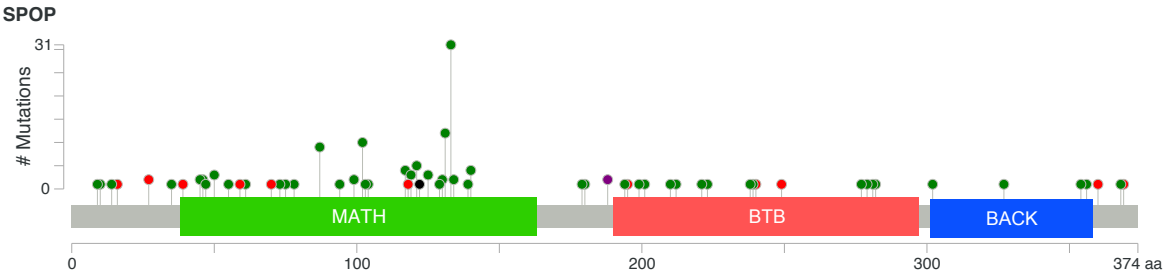

Appendix Figure S1. SPOP mutations are found in a number of cancer patient samples. The number of occurrences of mutations at specific SPOP residues in patients with cancer is shown (represented as colored pins above the notated SPOP domains). Missense mutations are shown as green pins. Alternative splicing, frame-shift deletions, and frame-shift insertions are shown as red pins. In-frame deletions are shown as black pins. Purple pins denote positions at which multiple types of mutations were observed (missense and a frame-shift deletion). The figure was generated from data compiled by cBioPortal (www.cBioPortal.org) (Gao *et al*, 2013; Cerami *et al*, 2012).

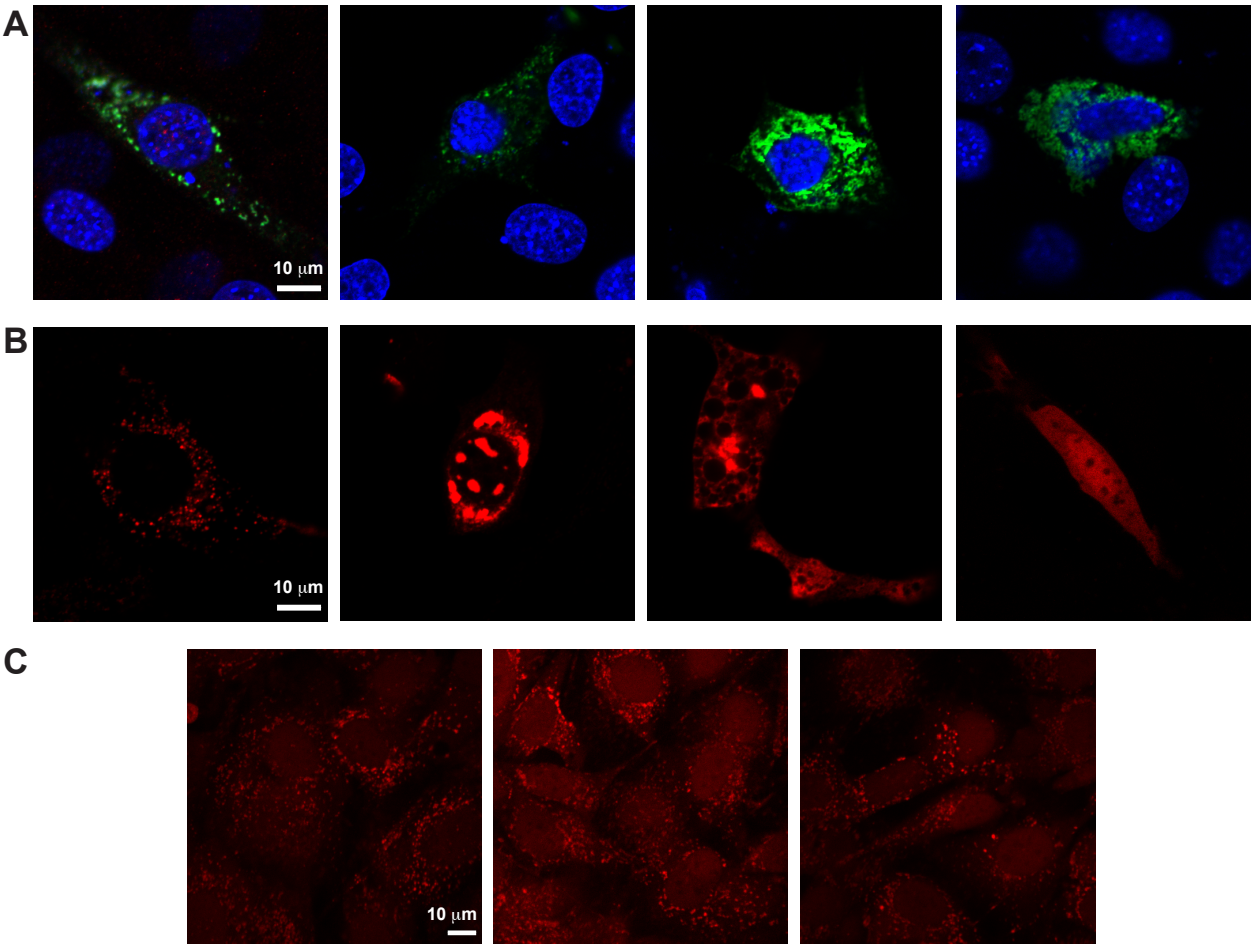

Appendix Figure S2. SPOP fusion constructs mislocalize in cells. (A) NIH 3T3 cells were transfected with GFP-SPOP (green) and fixed prior to imaging. Dual transfection with HA-SPOP (red) is shown in the first panel. DAPI (blue) marks the nucleus. **(B)** NIH 3T3 cells were transfected with mCherry-SPOP (red) and imaged. FRAP was preformed on the cytoplasmic puncta and no recovery was observed, suggesting the protein is aggregated. **(C)** NIH 3T3 cells were transfected with ReAsH-SPOP (red) and imaged. For all three fusion constructs, a lack of localization to nuclear speckles was observed.

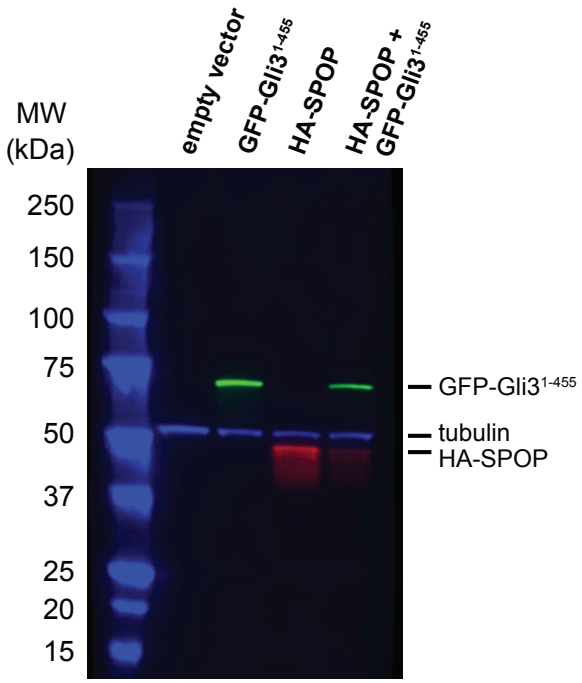

Appendix Figure S3: Expression levels of HA-SPOP and GFP-Gli3$^{1-455}$. NIH 3T3 cells were transfected with empty vector pcDNA, pcDNA GFP-Gli3$^{1-455}$, pcDNA-SPOP-HA, pcDNA-Gli3$^{1-455}$ + pcDNA-SPOP-HA. Two days post transfection, cells were lysed, equal amounts (~35 µg) of protein were loaded onto a gel, and western blotting was performed.

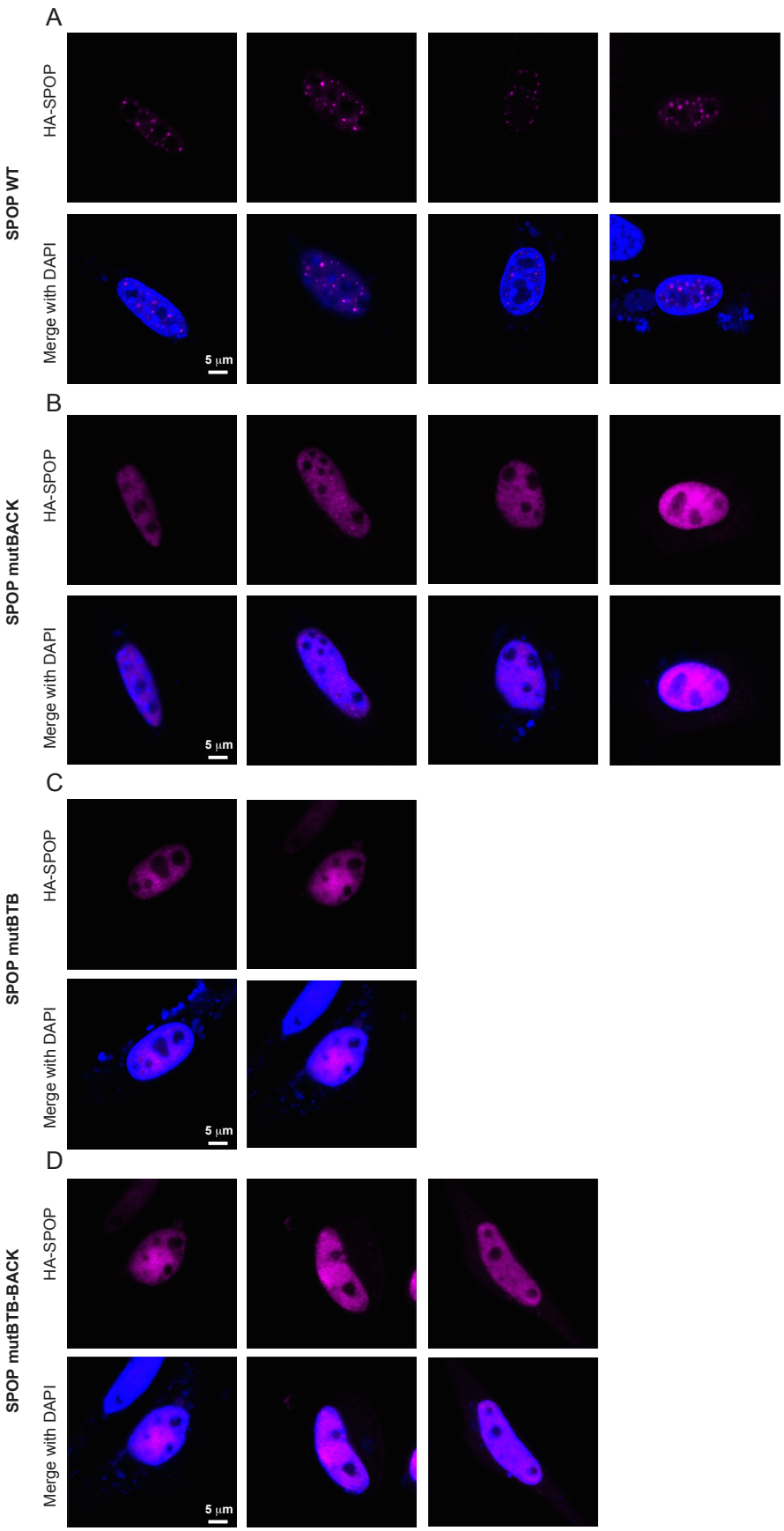
A
SPOP WT
HA-SPOP
Merge with DAPI
5 µm
B
SPOP mutBACK
HA-SPOP
Merge with DAPI
5 µm
C
SPOP mutBTB
HA-SPOP
Merge with DAPI
5 µm
D
SPOP mutBTB-BACK
HA-SPOP
Merge with DAPI
5 µm

Appendix Figure S4. SPOP mutants do not localize to nuclear speckles. Additional images showing diffuse nuclear localization of the SPOP mutants are presented. Representative data are shown in Figure 3.

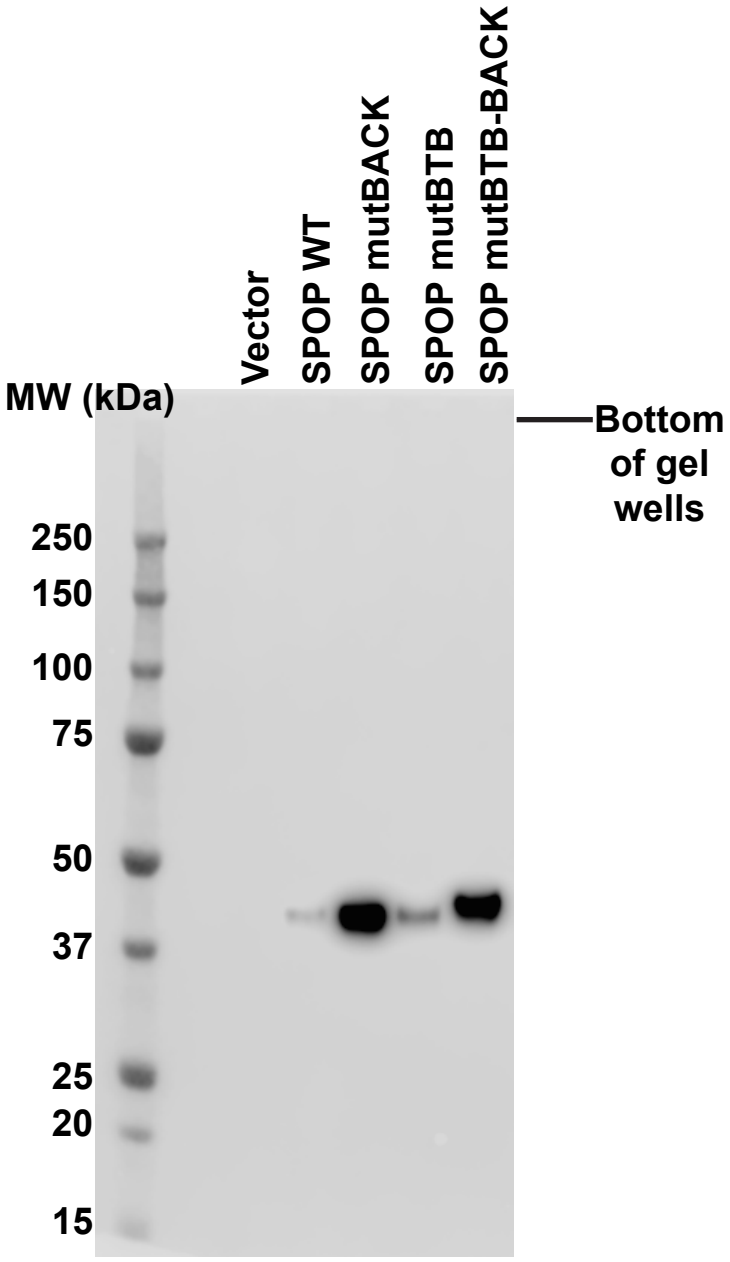

Appendix Figure S5. Crosslinking in cells recapitulates the phenotypes observed *in vitro*. Western blot of uncrosslinked samples showing that each SPOP construct is expressed in cells. These samples are from the same experiment presented in Fig 5C. HA-SPOP mutBACK and HA-SPOP mutBTB-BACK levels are higher than the others, explaining the different protein levels observed in the crosslinking experiments.

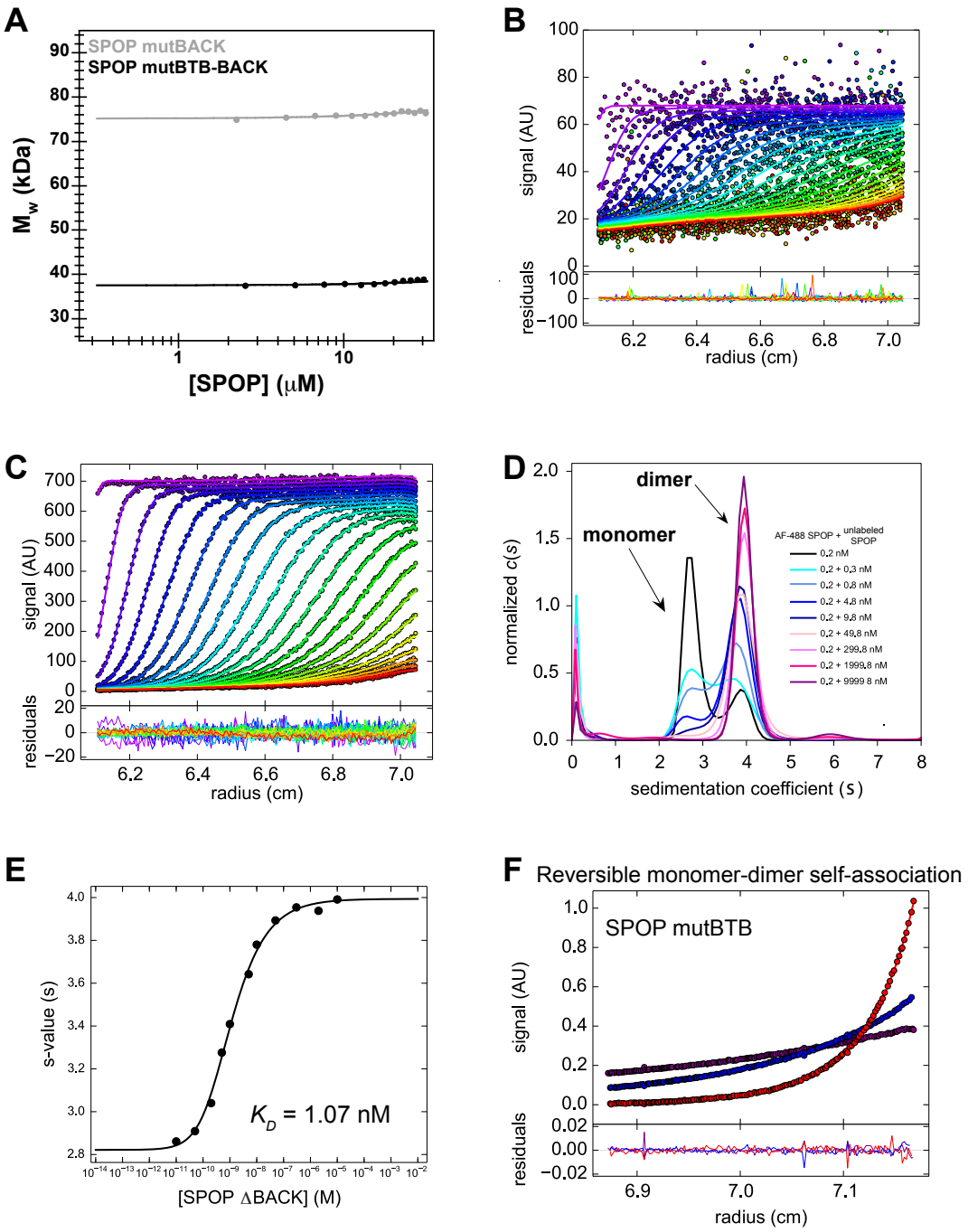

Appendix Figure S6. SPOP mutants do not form higher order oligomers and SV-AUC titration of AF488-SPOP ΔBACK with WT SPOP-ΔBACK. (A) Experimental weight-average molar mass (M_w) from CG-MALS for SPOP mutBACK (gray circles) and SPOP mutBTB-BACK (black circles) was fit to a monomer-dimer association model (gray line and black line, respectively). The residual monomer-dimer association observed (>500 μM, Figure 3 – table supplement 1) is likely due to domain interactions that are not completely abolished by the introduced mutations. Representative raw SV-AUC data for 50 pM **(B)** and 10 nM **(C)**

AF488-SPOP ΔBACK. **(D)** Sedimentation coefficient distributions of 0.2 nM AF488-SPOP ΔBACK titrated with WT SPOP ΔBACK are shown (concentrations given in figure). **(E)** The isotherm of the labeled/unlabeled SPOP ΔBACK titration series is shown. The weighted-average s-values were generated by integrating the data presented in panel **(D)** and were then plotted against total protein concentration. Points for 10 pM and 20 pM unlabeled SPOP (presented in Figure 2C) are also shown here to establish points at which only monomer is present. The data were fitted to a reversible monomer-dimer self-association model (solid line) yielding a K_D of 1.07 nM with a 95% confidence interval of [0.69, 1.66] nM. **(F)** Sedimentation equilibrium data for SPOP mutBTB were attained at a rotor temperature of 20°C at increasing rotor speeds of 9,000 (for 42 hours), 13,000 (for 32 hours) and 22,000 rpm (for 20 hours) (Zhao *et al*, 2013). Protein at concentrations of between 1.60 and 16.57 μM (130 μL) was loaded into double-sector centrepieces and absorbance distributions were recorded at 280 nm in 0.001 cm radial intervals with 20 replicates of each point. The data fit well to a monomer-dimer self-association model with a K_D of 32.5 μM [95% CI; 17.72-59.75] μM.

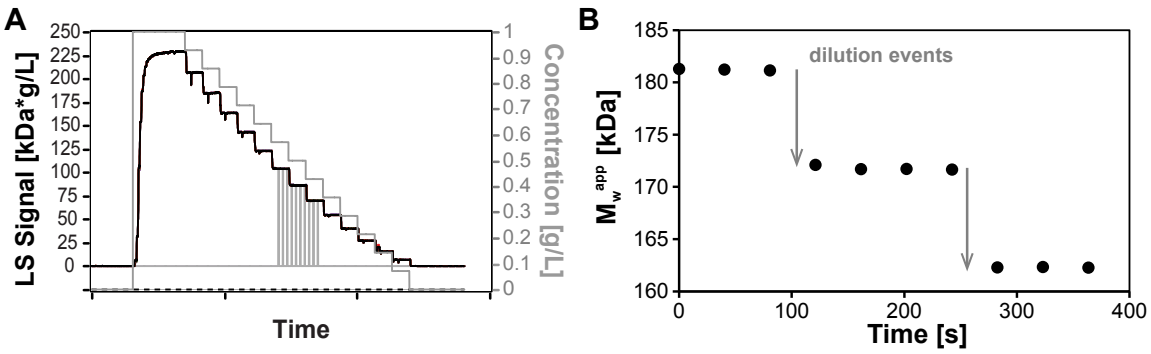

Appendix Figure S7. CG-MALS data are equilibrium measurements. (A) The light scattering signal (black) and nominal protein concentration (gray) are shown plotted against experimental time for a single SPOP$^{28\text{-}359}$ experiment. **(B)** Individual data points from distinct plateaus are shown. Vertical bars in panel **(A)** mark the positions of data points shown. These data show that equilibrium is rapidly reached for each plateau upon dilution of the protein solution and is maintained throughout monitoring of the light scattering signal during the course of the experiment.

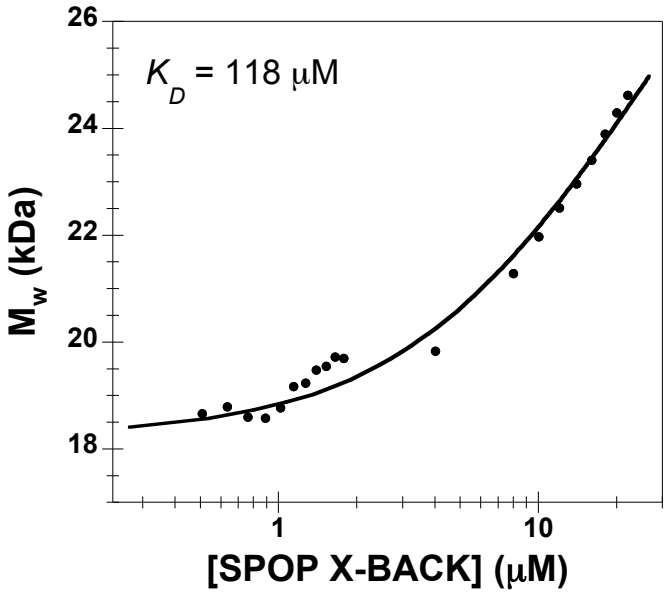

Appendix Figure S8. SPOP X-BACK forms dimers with decreased self-associaiton affinity. Experimental weight-average molar mass (M_w) from CG-MALS for SPOP X-BACK (black circles) was fit to a reversible monomer-dimer self-association model yielding a K_D of 118 μM (solid black line). This construct is similar in size to the construct used to crystallize the BACK domain (van Geersdaele *et al*, 2013) and contains a truncated BTB domain (self-association through the BACK domain only). We suspect that truncation of the BTB domain within this construct causes changes in the protein fold that have an effect on BACK-mediated self-association, explaining the increase in the observed K_D when compared to near full-length $SPOP^{28-359}$. Because of this difference in affinity, we propose that structures of SPOP containing all three domains may be required to truly represent the architecture of higher-order SPOP oligomers.

Appendix References

Cerami E, Gao J, Dogrusoz U, Gross BE, Sumer SO, Aksoy BA, Jacobsen A, Byrne CJ, Heuer ML, Larsson E, Antipin Y, Reva B, Goldberg AP, Sander C & Schultz N (2012) The cBio cancer genomics portal: an open platform for exploring multidimensional cancer genomics data. *Cancer Discov.* **2:** 401–404

Errington WJ, Khan MQ, Bueler SA, Rubinstein JL, Chakrabartty A & Privé GG (2012) Adaptor protein self-assembly drives the control of a cullin-RING ubiquitin ligase. *Structure* **20:** 1141–1153

Gao J, Aksoy BA, Dogrusoz U, Dresdner G, Gross B, Sumer SO, Sun Y, Jacobsen A, Sinha R, Larsson E, Cerami E, Sander C & Schultz N (2013) Integrative analysis of complex cancer genomics and clinical profiles using the cBioPortal. *Sci. Signal* **6:** pl1–pl1

Sakata E, Satoh T, Yamamoto S, Yamaguchi Y, Yagi-Utsumi M, Kurimoto E, Tanaka K, Wakatsuki S & Kato K (2010) Crystal structure of UbcH5b~ubiquitin intermediate: insight into the formation of the self-assembled E2~Ub conjugates. *Structure* **18:** 138–147

van Geersdaele LK, Stead MA, Harrison CM, Carr SB, Close HJ, Rosbrook GO, Connell SD & Wright SC (2013) Structural basis of high-order oligomerization of the cullin-3 adaptor SPOP. *Acta Crystallogr. D Biol. Crystallogr.* **69:** 1677–1684

Zhao H, Brautigam CA, Ghirlando R & Schuck P (2013) Overview of current methods in sedimentation velocity and sedimentation equilibrium analytical ultracentrifugation. *Curr. Protoc. Protein Sci.* **Chapter 20:** Unit20.12–20.12.49

Zheng N, Schulman BA, Song L, Miller JJ, Jeffrey PD, Wang P, Chu C, Koepp DM, Elledge SJ, Pagano M, Conaway RC, Conaway JW, Harper JW & Pavletich NP (2002) Structure of the Cul1-Rbx1-Skp1-F boxSkp2 SCF ubiquitin ligase complex. *Nature* **416:** 703–709

Zheng N, Wang P, Jeffrey PD & Pavletich NP (2000) Structure of a c-Cbl-UbcH7 complex: RING domain function in ubiquitin-protein ligases. *Cell* **102:** 533–539

Zhuang M, Calabrese MF, Liu J, Waddell MB, Nourse A, Hammel M, Miller DJ, Walden H, Duda DM, Seyedin SN, Hoggard T, Harper JW, White KP & Schulman BA (2009) Structures of SPOP-substrate complexes: insights into molecular architectures of BTB-Cul3 ubiquitin ligases. *Mol. Cell* **36:** 39–50